

CorrDetector: A Framework for Structural Corrosion Detection from Drone Images using Ensemble Deep Learning

Abdur Rahim Mohammad Forkan^{a,*}, Yong-Bin Kang^b, Prem Prakash Jayaraman^a, Kewen Liao^{a,c}, Rohit Kaul^a, Graham Morgan^d, Rajiv Ranjan^d, Samir Sinha^e

^a*Department of Computer Science and Software Engineering, Swinburne University of Technology, Melbourne, Victoria, Australia*

^b*Department of Media and Communication, Swinburne University of Technology, Melbourne, Victoria, Australia*

^c*Discipline of Information Technology, Peter Faber Business School, Australian Catholic University, Sydney, NSW, Australia*

^d*Newcastle University, Newcastle upon Tyne, NE1 7RU, UK*

^e*Robonomics AI, York Street, Sydney, NSW, Australia*

Abstract

In this paper, we propose a new technique that applies automated image analysis in the area of structural corrosion monitoring and demonstrate improved efficacy compared to existing approaches. Structural corrosion monitoring is the initial step of the risk-based maintenance philosophy and depends on an engineer's assessment regarding the risk of building failure balanced against the fiscal cost of maintenance. This introduces the opportunity for human error which is further complicated when restricted to assessment using drone captured images for those areas not reachable by humans due to many background noises. The importance of this problem has promoted an active research community aiming to support the engineer through the use of artificial intelligence (AI) image analysis for corrosion detection. In this paper, we advance this area of research with the development of a framework, **CorrDetector**. **CorrDetector** uses a novel ensemble deep learning approach underpinned by convolutional neural networks (CNNs) for structural identification and corrosion feature extraction. We provide an empirical evaluation using real-world images of a complicated structure (e.g. telecommunication tower) captured by drones, a typical scenario for engineers. Our study demonstrates that the ensemble approach of **CorrDetector** significantly outperforms the state-of-the-art in terms of classi-

*Corresponding Author

Email addresses: fforkan@swin.edu.au (Abdur Rahim Mohammad Forkan), ykang@swin.edu.au (Yong-Bin Kang), pjayaraman@swin.edu.au (Prem Prakash Jayaraman), Kewen.Liao@acu.edu.au (Kewen Liao), rkaul@swin.edu.au (Rohit Kaul), graham.morgan@newcastle.ac.uk (Graham Morgan), raj.ranjan@ncl.ac.uk (Rajiv Ranjan), samir@robonomics.ai (Samir Sinha)

fication accuracy.

Keywords: Corrosion detection, Object detection, Deep Learning, Drone Images, Industrial structure, Ensemble model, CNN.

1. Introduction

Inspecting faults (e.g. corrosion) is a major problem in industrial structures such as building roofs, pipes, poles, bridges, and telecommunication towers [1]. This is a vital service for several industrial sectors, especially manufacturing, where structures (assets) that are subject to corrosion due to their exposure to the weather are used to deliver critical products or services. The problem of corrosion may cost Australia up to \$32 billion annually, which is greater than \$1500 for every Australian each year [2]. Corrosion is not simply a financial cost if left unattended; the endangerment of lives may also be a real risk. Without adopting to the latest in AI-driven solutions, businesses are losing millions in time and money to identify corrosion using methods that have changed little with heavy reliance on human judgement [3]. The timely and accurate detection of corrosion is a key way to improve the efficiency of economy by instigating appropriately managed maintenance processes that will also save lives.

A fast and reliable inspection process for corrosion can ensure industrial assets are maintained in time to prevent regulatory breaches, outages or catastrophic disasters. In most cases, inspections of such assets are conducted manually which can be slow, hazardous, expensive and inaccurate. Recently, drones have proven to be a viable and safer solution to perform such inspections in many adverse conditions by flying up-close to the structures and take a very large number of high-resolution images from multiple angles [4]. The images acquired through such process are stored and then subsequently reviewed manually by expert engineers who decide about further actions. However, this causes a problem of plenty for highly qualified engineers to manually identify corrosion from the images which further leads to a high level of human error, inconsistencies, high lead time and high costs in terms of man-hours.

Existing approaches for identifying structural corrosion from images are either based on Computer Vision (CV) [5] or Deep Learning (DL) techniques [6, 7]. In recent CV-based techniques [8], non-trivial prior knowledge and extensive human efforts are required in designing high quality corrosion features from images. In addition, one cannot hope much on the performance (or the accuracy of corrosion detection) in the case that the corrosion features are somewhat incorrectly identified. Compared with computer vision/image processing [9] and vanilla machine learning approaches [10], DL-based methods, in particular Convolutional Neural Networks (CNNs) [11, 12] have shown the ability to automatically learn important features, outperforming state-of-the-art vision-based approaches [6, 7, 13] and achieving human-level accuracy.

In this paper, we present a Deep Learning (DL)-based framework named **CorrDetector**, for detecting corrosion from high resolution images captured by

drones. As the key innovation, we propose and develop an ensemble of CNN models [14] which is capable of detecting corrosion in target structure (i.e. object) from such high resolution images at significantly higher accuracy than the current state-of-the-art CNN models. More specifically, the proposed framework is capable of providing i) industrial structure recognition - detect the industrial structure (i.e. object of interest) in the image captured by the drone (since the drone image is captured in a real-world environment that is filled with background noise) and; iii) localised detection of corrosion - detect which areas in the industrial structure contains corrosion. Most DL-based solutions for corrosion detection use image samples captured by DSLR (digital single-lens reflex), digital or mobile cameras with human involvement in taking pictures [7, 15] in more controlled environment. Such image samples are much lower in resolution than drone images. Moreover, these samples can be biased as they are captured specifically to be utilised for experimental purposes at certain distances and angles. Therefore, such images comprised of human judgements to focus in specific type of corrosion area within the image which can be easily isolated and distinguishable even in visual inspection [7]. Moreover, previous studies have mostly focused on corrosion identification only in metallic surfaces [4, 6, 7, 10]. To the best of our knowledge, this work is the first attempt that utilises real-world high-resolution unaltered images captured by drones in industrial and real-world settings to identify corrosion in industrial structure such as telecommunication tower. More specifically, this paper makes the following contributions:

- Present a novel framework, **CorrDetector** with a 4-layer architecture to detect industrial object and identify regions of corrosion in high-resolution images of industrial assets captured by drones in a real-world setting from various positions, angles and distances.
- Present an innovative ensemble approach that combines two deep learning models; a deep learning model for recognising and separating targeted industrial structure from the background and a deep learning model to identify corrosion in specific regions of the industrial structure (localised).
- Present a systematic methodology for training our ensemble model using high-resolution drone images that includes two types of annotation techniques namely grid-based and object-based.
- A comprehensive evaluation using a real-world dataset (high resolution drone images of telecommunication towers) and comparison with current state-of-the-art deep learning models for corrosion detection to demonstrate the efficacy of the proposed **CorrDetector**.

The rest of the paper is organised as follows. Section 2 provides a discussion of current state-of-the-art in corrosion detection from images. Section 3 presents the systematic methodology for developing an ensemble of CNN models for corrosion detection. Section 4 presents the experimental domain, the empirical evaluation and a comprehensive analysis of our proposed approach against the current-state-of-the-art and finally Section 5 concludes the paper.

2. Related Works

The most recent research identify the possibility of the utilisation of computer vision (CV) [16] coupled with deep learning (DL) [17] for defect identification. This has been proven in the literature to be capable of identifying corrosion in building structures. As this may lower the opportunity of human error while greatly speeding up the analysis process there has been a significant increase in active research pursuing approaches based on these two cornerstones.

Several CV-based approaches have been proposed for identifying defects in industrial structures to aid in civil engineering maintenance life-cycle service. In particular, structures prone to corrosion through repeated erosion may result in loss of life (e.g., flight, at-sea) and are particular drivers for such work.

Authors in [5, 18] used wavelet transforms on images to detect structural corrosion. Assuming images are obtained through nondestructive imaging (NDI) of ageing aircraft materials and structures, the work in [18] attempts to identify damage on ageing aircraft structures. Wavelet analysis was used for feature extraction, a clustering technique is used for damage segmentation, and a K-means distance-based method is used for damage classification. [5] used wavelet features and the Shannon entropy method for detecting damages in ship hulls.

The work in [19] focuses on corrosion surface damage identification in the form of pitting and micro-cracks in metal using an image analysis based on wavelet transforms. The work [20] uses camera based image analysis techniques to identify, quantify and classify damage in aluminium structures. The proposed techniques used the optical contrast of the corroded region with respect to its surroundings, performed edge detection techniques through image processing approaches and computed each region to predict the total area of the affected part. Authors in [10] adopted color space features and J48 decision tree classification for detecting rust in steel bridges. They obtained high accuracy (97.51%) but only used a total of 165 images. Overall, in all CV-based approaches the focus is on feature extraction techniques rather than classification whereas in a DL-based solution using convolutional neural networks (CNNs) there is an opportunity for automatic feature extraction that may lead to more optimum and adaptable learning strategies. This provides an opportunity for a broader area of subject matter to be considered by a single approach (coupled with transferred learning [11]) as corrosion types are different as can be seen in the related works just described.

Within the domain of inspecting industrial structures, Authors in [6] adopt ‘Faster R-CNN’ for detecting cracks in metal objects. Their database contains 2366 images (with 500×375 pixels) labelled with five types of damages - concrete crack, steel corrosion classed as medium or high, bolt corrosion, and steel delamination. To develop a training set, 297 images (with a resolution of $6,000 \times 4,000$ pixels) were collected using a Nikon D5200 and D7200 DSLR cameras. Images were taken under different lighting conditions. Their evaluation results showed 90.6%, 83.4%, 82.1%, 98.1%, and 84.7% average precision (AP) ratings for the five damage types respectively with a mean AP of 87.8%. The traditional CNN based method showed high accuracy in this and their previous work [15].

For the task of corrosion detection, the work in [7] applied two CNN networks (ZF Net and VGG). However, the authors focused on the computational aspects by proposing two shallow CNN architectures ‘Corrosion7’ and ‘Corrosion5’. These two networks were shown to be similar to ZF and VGG in terms of detection performance. Taking a closer look at the work of [7], during its training phase, authors used color spaces (RGB, YCbCr, CbCr, and grayscale). After determining the optimal color space, they identified that CbCr to be the most robust for corrosion detection using wavelet decomposition. Using the chosen color space, CbCr, authors proposed CNN architectures with a sliding window using different sizes (i.e. 32x32, 64x64, and 128x128). This sliding window approach was used to detect corroded areas within an image. The authors achieved 96.68% mean precision using 926 images. However, they only focus on clearly visible surface images whereas, our image samples are from a complicated industrial structure. Other corrosion detection model using deep learning did not obtain accuracy over 88% using the test dataset of targeted industrial assets [4, 13].

The approaches described in the literature rely on CNN approaches that could be advanced by bringing together techniques. Indeed, the transfer learning of the CNN is already established as a technique with learning images constructed efficiently through the transfer of knowledge [11]. We considered the possibility of an ensemble technique, using the latest CNN approaches that provide pixel level masking for object identification (Mask R-CNN [21]) together with localised corrosion detection. Such ensemble approach for corrosion detection differs from existing work in the literature since the image samples are captured in a controlled setting (i.e. images are captured for the purpose of empirical evaluations). On contrary, our proposed approach works on unaltered drone images collected in a real-world setting (via a drone used by engineers to manually assess structural corrosion) which presents high level of complexity (such as filled with background noise, includes complex industrial structure and captured at different angles, distance and different times of the day i.e overcast, sunny etc.).

3. The CorrDetector Framework

The architecture of **CorrDetector** framework is illustrated in Figure 1. In Data acquisition layer, a large number of images of the targeted industrial structure (e.g. building roofs, telecommunication towers, bridges, poles, wires and pipelines) are acquired through human-operated drones with advanced cameras. Using these images, engineers identify areas of defects (e.g. corrosion) by visual inspection. The human expert annotated images using various annotation software tools are utilised in data preparation layer.

CorrDetector incorporates two types of annotations. Given an image, the first type is the *grid-based annotation* where the multiple small rectangular

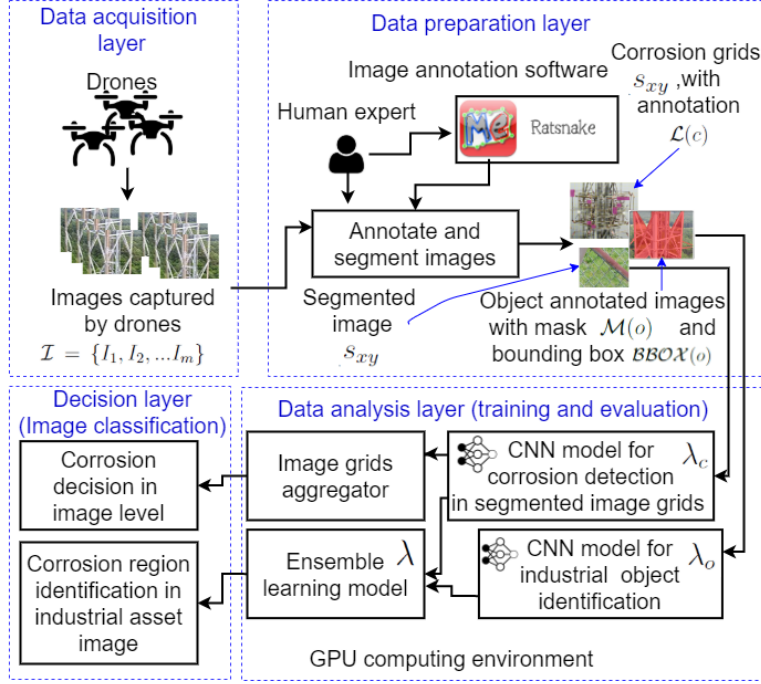


Figure 1: The architecture of the **CorrDetector** framework

grids (or segments)¹ in the image are drawn. Then, a human expert annotates each of these grids with corrosion or non-corrosion, depending on the fact that the grid contains corroded structural component(s). The grids are separated using image processing techniques. These annotations are used to build ground truth information for corrosion detection deep learning model in **CorrDetector**. Another type of the annotation is the *object annotation*, where a human expert uses an image annotation tool to create a polygonal mask annotation around the target object (e.g. a telecommunication tower on which corrosion needs to be detected). The annotated data are used to train an object recognition model in **CorrDetector**.

In data analysis layer, two deep learning models using different CNNs are learned to develop an ensemble model in **CorrDetector**. These models are denoted as λ_c and λ_o that will be used for grid-based corrosion detection and industrial object identification, respectively. The *image grids aggregator* is used to combine all segments (or grids) within the target image to predict whether there is corrosion or not in the image. As another key model, **CorrDetector** also incorporates, an ensemble model, denoted as λ , that takes the outputs

¹In this paper, to simplify the presentation, we interchangeably use the terms, grid and segment.

predicted by the λ_c and λ_o as the input, and predict which structural objects has corrosion or not. This ensemble approach aims to improve our prediction capability by predicting corrosion on only the structural components.

The decision layer makes the final two decisions for a given unknown image. The first decision is the outcome that contains corrosion or not in the image. The decision is made by aggregating outcomes of individual segments estimated using λ_c for that image. The other decision is about which regions of industrial object are likely to have corrosion in the image. This is done using the ensemble model, λ . The corrosion regions can be visualised as highlighted rectangular grids.

3.1. Image annotation methodology

In this section we present the image annotation methodology employed by **CorrDetector** in the *data preparation layer*.

Let $\mathcal{I} = \{I_1, I_2, \dots, I_m\}$ be list of m images captured by drones in the data acquisition layer. Each image $I_{i \in [1, m]}$, has a $W \times H$ resolution.

In our work, given an image, image annotation means annotating the image with a caption that best explains the image based on the prominent objects present in that image and to make the objects recognisable for machines. The annotation is done by humans manually using image annotation tools to create the ground truth data for **CorrDetector**. An image having places of corrosion is annotated with a cropped bounding box so that other parts of the image can be considered as with no corrosion. As described previously, we apply two types of annotation, grid-based annotation and object annotation on each image, I_i .

3.1.1. Grid-based image annotation

The objective of the grid-based corrosion detector, λ_c is to predict whether a region in a given image with has corrosion or not. Thus, we formulate the prediction problem for λ_c as a binary (1/0) classification, where 1 means corrosion and 0 otherwise. For this kind of classification, the *image segmentation* approach has been proven useful [22]. In this approach, a given original image (in our case, each $I_i \in \mathcal{I}$), it is segmented equally to a number of rectangular grids. Then, each of the grids is annotated with 1 meaning corrosion, and 0 meaning non-corrosion. This is also a kind of data upsampling or augmentation approach to create enough data to train CNN models.

In our approach, human experts use an image annotation tool to split each image I_i into $n \times n$ rectangular grids. Then, each grid, s_{xy} (where $1 \leq x, y \leq n$) having corrosion in industrial structures is annotated, producing the grid-based annotated image, I_i^c . All the grids in I_i^c , which are not annotated with corrosion, are considered as non-corrosion grids. The image set produced from original image set \mathcal{I} in this layer is denoted as $\mathcal{I}^c = \{I_1^c, I_2^c, \dots, I_m^c\}$.

3.1.2. Object annotation

Our goal here is to indicate which are parts of industrial component objects given an image, separating them from unimportant noises (e.g. background images - trees) in a given image. This process is known as background separation.

By doing so, we desire to focus on identifying corrosion only on the objects related to the target industrial objects. The annotated data of this step are used to learn λ_o to detect objects associated with industrial structures.

There are two popular annotation approaches used for object separation. The bounding box [23] is the most commonly used approach for such purpose. This basically highlights an object in an image with a rectangular box to make it recognisable for machines. The example of this annotation is shown in Figure 2(a). Another approach is polygonal segmentation [23] which is used to annotate objects with irregular shapes, that is, polygons. Unlike bounding boxes, this approach can exclude unnecessary objects around the target structural objects. Polygons are more precise when it comes to localisation. The example is presented in Figure 2(b).

Our targeted industrial structures have complex and irregular structure and therefore we use the polygonal annotation approach. Given an image, a human expert creates polygonal annotations around each of the target structure objects. Let the annotated image corresponding to a given image I_i be I_i^o . Let \mathcal{M}_i be the polygonal mask (see Figure 2(b)) and $\mathcal{BB}\mathcal{O}\mathcal{X}_i$ be the bounding box information (see Figure 2(a)) for I_i^o . The image set produced after this step from original image set \mathcal{I} is $\mathcal{I}^o = \{I_1^o, I_2^o, \dots, I_m^o\}$.

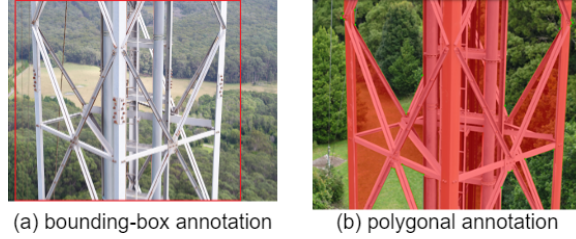


Figure 2: Object annotation methods

3.2. Processing of annotated images

Given the image set \mathcal{I} , we have now obtained the corresponding grid-based annotated and object annotated image sets in the data preparation layer. We denoted these sets as \mathcal{I}^c and \mathcal{I}^o , respectively. These image sets are used to build our CNN models: λ_c , λ_o and final ensemble model λ in **CorrDetector**.

3.2.1. Corrosion Image Segmentation and Separation (CISS) algorithm

Out of m images in \mathcal{I} , k images are randomly sampled to be in a training set, while the rest $m - k$ forms the rest (k is a whole number). The same k images are picked from \mathcal{I}^o and \mathcal{I}^c where, image I_i^o is the object annotated version and image I_i^c is grid annotated version for image I_i . To develop λ_o we use k images in \mathcal{I}^o denoted by, \mathcal{T}_{λ_o} . Similarly, for λ_c k images used from \mathcal{I}^c for training is denoted by \mathcal{T}_{λ_c} .

Given an image I_i , its corresponding grid-based annotation image I_i^c contains $n \times n$ rectangular grids. Each grid (or segment), s_{xy} is a cropped image

with the dimension $w \times h$ (where $w = W/n$ and $h = H/n$) of I_i which have $W \times H$ dimension. The annotated information in I_i^c produces a binary matrix $B_i = [b_{xy}]$ of dimension $n \times n$ where $1 \leq x, y \leq n$. The binary decision for b_{xy} is obtained as,

$$b_{xy} = \begin{cases} 1 & s_{xy} = \mathcal{L}_c \\ 0 & s_{xy} \neq \mathcal{L}_c \end{cases} \quad (1)$$

That is, $b_{xy} = 1$ if the grid of the x -th row and y -th column is annotated as corrosion, and $b_{xy} = 0$, otherwise. Here \mathcal{L}_c represents annotation for corrosion. By applying Equation 1 to all grids in the image I_i^c , we create the binary matrix $B_i = [b_{xy}]$. Therefore, for m images in \mathcal{I} (where $m = |\mathcal{I}|$), we obtain the list of m binary matrices, $\mathcal{B} = \{B_1, B_2, \dots, B_m\}$.

We developed *Corrosion Image Segmentation and Separation (CISS)* algorithm for generating training data, \mathcal{T}_{λ_c} for corrosion detection model, λ_c . The steps of image segmentation and training data separation process is described in Algorithm 1.

Algorithm 1 CISS Algorithm

Input: $\mathcal{I}^c = \{I_1^c, I_2^c, \dots, I_i^c, \dots, I_k^c\}$; $\mathcal{B} = \{b_1, b_2, \dots, b_i, \dots, b_k\}$

Output: Training set for λ_c , \mathcal{T}_{λ_c}

```

 $\mathcal{S}_c \leftarrow \phi$  ;  $\mathcal{S}_{nc} \leftarrow \phi$ 
for  $i = 1$  to  $k$  do
     $S_i = \{s_{xy} : 1 \leq x, y \leq n\} \leftarrow \text{segment}(I_i^c)$ 
    for each  $s_{xy} \in S_i$  do
        retrieve  $b_{xy}$  from  $B_i$ 
        if  $b_{xy} = 1$  then
             $\mathcal{S}_c \leftarrow \mathcal{S}_c \cup \{s_{xy}\}$ 
        end
        else
             $\mathcal{S}_{nc} \leftarrow \mathcal{S}_{nc} \cup \{s_{xy}\}$ 
        end
    end
 $N_c \leftarrow |\mathcal{S}_c|$ 
shuffle all segments  $s_{nc} \in \mathcal{S}_{nc}$ 
 $\hat{\mathcal{S}}_{nc} \leftarrow \text{random } 2 \times N_c \text{ segments from } \mathcal{S}_{nc}$ 
 $\mathcal{S} \leftarrow \mathcal{S}_c \cup \hat{\mathcal{S}}_{nc}$ 
 $\mathcal{T}_{\lambda_c} \leftarrow \text{shuffle}(\mathcal{S})$ 
return  $\mathcal{T}_{\lambda_c}$ 

```

In Algorithm 1, our defined function, $\text{segment}(I_i)$ generates $n \times n$ segmented images from I_i . That is,

$$I_i \rightarrow S_i = \{s_{xy} : 1 \leq x, y \leq n\} \quad (2)$$

In total, the number of segmented images produced from m images is $m \times n \times n$.

The segments of all k images are combined and then randomly shuffled. Since the corrosion mainly resides in the industrial structure within an image, the number of identified segments having \mathcal{L}_c , N_c is much smaller than the number of non-corrosion segments, N_{nc} (e.g. only 16% in overall distribution for a real-world use case). To avoid this imbalance issue, all corrosion segments (\mathcal{S}_c) are selected for model development. Then a random samples of non-corrosion segments (\mathcal{S}_{nc}) are chosen such that the selected number of non-corrosion segments $N_{nc} = 2 \times N_c$. This produces the final non-corrosion image segment set $\hat{\mathcal{S}}_{nc}$. In the end, \mathcal{S}_c and $\hat{\mathcal{S}}_{nc}$ are combined and shuffled which produces the final image set \mathcal{T}_{λ_c} which is used as the input image set for λ_c .

3.3. CorrDetector CNN models development

The **CorrDetector** framework incorporates the following models that have been developed for detecting corrosion in images of industrial structures. In the rest of this section, we provide detailed descriptions of the model development process.

- λ_c : Given the training set, \mathcal{T}_{λ_c} containing random $3 \times N_c(N_c + 2 \times N_c)$ image segments from \mathcal{I}^c . Each segment s_{xy} belongs to \mathcal{T}_{λ_c} as described in Algorithm 1. The objective of λ_c is to automatically identify segments s_{xy} having \mathcal{L}_c in each of $m - k$ images in \mathcal{I} and compare with the ground truth \mathcal{L}_c in same $m - k$ images in \mathcal{I}^c .
- λ_o : Given the training set, \mathcal{T}_{λ_o} containing k images from \mathcal{I}^o . Each $I_i^o \in \mathcal{I}^o$ is annotated with target object T . The objective of λ_o is to automatically estimate $\hat{\mathcal{M}}_o$ in $m - k$ images in \mathcal{I} and compare with the ground truth \mathcal{M}_o in same $m - k$ images in \mathcal{I}^o .
- λ : Given the outcome of λ_c and λ_o . The objective of ensemble model, λ is to estimate corrosion for each individual segments s_{xy} in a test image I_i such that s_{xy} is detected as a corrosion segment by λ_c and the presence of targeted object is detected in s_{xy} by λ_o .

3.3.1. CNN model for corrosion detection in image segment-level, λ_c

Our proposed CISS algorithm generates multiple rectangular segments (s_{xy}) of the complete image. Each segment represents a smaller size image. Therefore, for detecting corrosion in such small image, the CNN mainly needs to learn the features for the corrosion color. A simple CNN can serve such purpose.

In general, a CNN consists of multiple convolution (CO) and pooling layers followed by the fully connected (FC) and classification layers. CO are used to extract features from the training images. CO consists of kernels (a set of small receptive fields). The weight values for the kernels are typically initialised with random values and updated during training. Pooling layers are used to decrease the data to decrease the computational costs during the training phase. There are two well-known methods in pooling: (1) max pooling (MP) and (2) mean pooling (MeP).

The goal of designing a simple CNN is to determine whether such CNN model can be used to predict corrosion in a good performance. Thus, to construct λ_c , we propose a shallow version of VGG16 [24] with 5 layers - 3 convolution (CO) layers and 2 fully-connected (FC) layers (see Table 1. Our model is inspired by the approach proposed in [7] where they proposed a 7-layer CNN called Corrosion7 (see Table 2).

Table 1: λ_c architecture - CO:convolution, MP: Max Pooling, KS: Kernel Shape, NK: Number of Kernels, NV: Number of Variables. Each number indicate a layer number.

Layer	Input	MP	KS	NK	NV
CO1	224 X 224 X3	2 X 2	3 X 3	32	288
CO2	224 X 224 X 32	2 X 2	3 X 3	64	576
CO3	64 X 64 X 64	2 X 2	3 X 3	128	1152
FC1	2 X 2 X 128	-	512	128	65536
FC2	128	-	128	2	128

Table 2: Corrosion7 architecture

Layer	Input	MP	KS	NK	NV
CO1	128 X 128 X 3	64 X 64	3 X 3	58	8526
CO2	33 X 33 X 58	17 X 17	3 X 3	128	185600
CO3	9 X 9 X 128	9 X 9	3 X 3	192	221184
CO4	9 X 9 X 192	-	3 X 3	192	331776
CO5	9 X 9 X 192	-	3 X 3	128	221184
FC1	4 X 4 X 128	-	512	1024	2097152
FC2	1024	-	128	2	2048

After constructing λ_c the following steps are performed,

1. λ_c is trained with the training set, \mathcal{T}_{λ_c} generated in CISS Algorithm (Algorithm 1).
2. The trained λ_c is tested with $m - k$ images in \mathcal{I}^c .
3. For a given test image, $I_i \in \mathcal{I}$, λ_c generates decision for \mathcal{L}_c using confidence value $conf(s_{xy})$ for each $n \times n$ rectangular segments, s_{xy} in I_i where $0 \leq conf(s_{xy}) \leq 1$.
4. Let $\mathcal{CS}_i = [conf(s_{xy})]$ be the confidence matrix for I_i , for $m - k$ images λ_c generates, $\mathcal{CS} = \{\mathcal{CS}_1, \mathcal{CS}_2, \dots, \mathcal{CS}_i, \dots, \mathcal{CS}_{m-k}\}$.
5. The decisions for \mathcal{L}_c for all segments s_{xy} in I_i produce binary matrix $\hat{B}_i = [\hat{b}_{xy}]$ where each \hat{b}_{xy} is computed according to Equation 1. We call this segment-level prediction (SLP). $\hat{\mathcal{B}} = \{\hat{B}_1, \hat{B}_2, \dots, \hat{B}_i, \dots, \hat{B}_{m-k}\}$.
6. The overall confidence for image I_i is computed as,

$$conf_c(I_i) = \frac{\sum_{x=1}^n \sum_{y=1}^n \hat{b}_{xy}}{n \times n} \quad (3)$$

These confidence values, $\mathcal{CC} = \{conf_c(I_1), conf_c(I_2), \dots, conf_c(I_i), \dots, conf_c(I_{m-k})\}$ are used to make decision for image-level (IL) prediction for corrosion.

3.3.2. CNN model for Industrial object identification, λ_o

We have used Mask R-CNN [21] for developing the model for object identification, λ_o . This is one of the best performing model in object detection and instance segmentation [21]. For a given image, I_i , this network can separate different objects. In our industrial object identification problem we have only one target object. Mask R-CNN provides output for the object bounding boxes, classes and masks. There are two stages of Mask R-CNN (region proposal network and neural network) and both of them are connected to a backbone network.

The backbone network for Mask R-CNN is a deep neural network which is responsible for extracting features from raw image. The deeper network may result higher accuracy, however, can highly impact on the duration of model training and classification. By passing through backbone network, images are converted into feature maps. A top-down pyramid structure, Feature Pyramid Network (FPN) [25] is used to extract features. The extracted features from top layers are transferred to lower layers. Due to this structure each layer in pyramid has access to the higher and lower layers. In this context, we have used ResNet-101 FPN backbone as feature extractor for our Mask R-CNN to increase its speed and performance.

The first stage of Mask R-CNN is a light weight neural network called (RPN) that generates regions of interest (RoIs) from feature maps provided by backbone network [21]. The second stage is another neural network takes proposed RoIs by the first stage and assign them to several specific areas of a feature map level, scans these areas, and generates objects, bounding boxes and masks. There is a branch for generating masks for each objects in pixel level. It also provides the confidence value of detected bounding box similar to Faster R-CNN.

After constructing the Mask R-CNN model with backbone network ResNet-101, λ_o , the following steps are performed.

1. λ_o is trained with training set, \mathcal{T}_{λ_o} containing k images from \mathcal{I}^o .
2. The trained λ_o is then tested with remaining $m - k$ images in \mathcal{I}^o .
3. For a given test image, $I_i \in \mathcal{I}$, λ_o generates output of the estimated mask of target object, $\hat{\mathcal{M}}_{o_i}$ with a confidence value $conf_o(I_i)$. $conf_o(I_i)$ is used to make decision for object detection for I_i and $0 \leq conf_o(I_i) \leq 1$.
4. The test result for all $m - k$ images in \mathcal{I} finally generates the list of images containing $\hat{\mathcal{M}}_{o_i}$ estimated by λ_o , $\hat{\mathcal{I}}_{m-k}^o$ and the list of their confidence values, $\mathcal{CO} = [conf_o(I_i)]_{i=1}^{m-k}$

3.3.3. Ensemble model for region-based corrosion detection, λ

The Ensemble model, λ is a machine learning model that utilises the outcome from λ_c and λ_o to make the final decision for corrosion in an image segment (i.e. region of an image). Figure 3 shows the process of development of the ensemble

model λ from the outcomes of λ_c and λ_o . An example of a CNN structure for corrosion detection in an image segment is also presented in the bottom part of the figure.

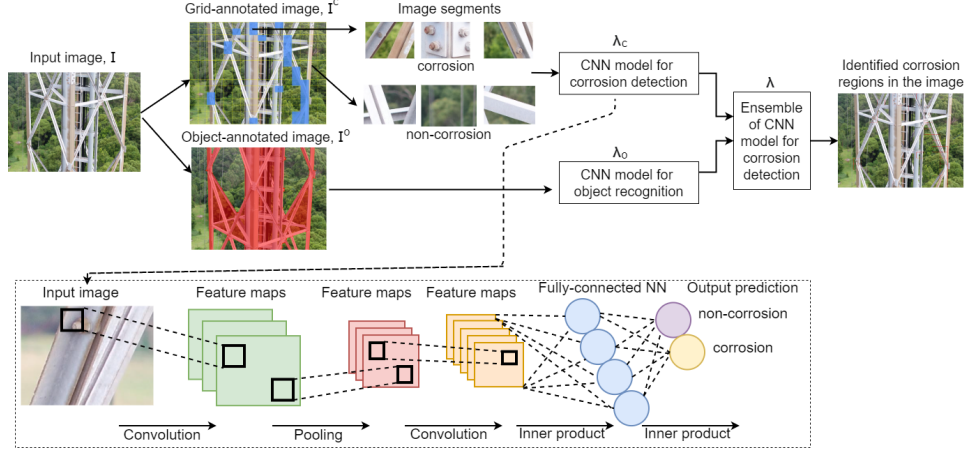


Figure 3: An ensemble DL model with an overview CNN structure for corrosion detection

Algorithm 2 outlines the steps involved in our proposed Ensemble Region-based Corrosion (ERC) detection.

The steps of Algorithm 2 are discussed as follows

- The algorithm generates 2 different feature set, FC and FB , using confidence values and binary decision values of each predicted image segment s_{xy} by λ_c respectively.
- The $flatten(X)$ function converts $n \times n$ matrix X to n^2 elements single dimensional array.
- To convert the mask outcome of λ_o , \mathcal{M}_o to a binary matrix similar to the outcome of λ_c . We first convert the masked outcome of image, I_i into same $n \times n$ segments. Then we compute whether a segment belongs to the detected object using the area of intersection of the segment and object mask.
- We consider a segment is part of the object, if object mask overlap with more than 10% area of the segment. If the condition is true we assign value 1 and 0, otherwise. Here, we ignore a small amount of of overlap (10%) based on the observation that if that part of this object contains corrosion that should be detected in remaining 90% overlapped with other segments.
- Finally, we combine this binary outcome of λ_o with λ_c and true label which produce the feature set, FB .

Algorithm 2 ERC Algorithm

Input: \hat{I}_{m-k}^o ; \mathcal{CO} ; \mathcal{B} ; $\hat{\mathcal{B}}$; \mathcal{CS} **Output:** Training set for λ : FC and FB $FB \leftarrow \phi$; $FC \leftarrow \phi$ **for** each $\hat{I}_i^o \in \hat{I}_{m-k}^o$; $B_i \in \mathcal{B}_{m-k}$; $\hat{B}_i \in \hat{\mathcal{B}}$; $conf_o(I_i) \in \mathcal{CO}$; $\mathcal{CS}_i \in \mathcal{CS}$ **do** $\bar{B}_i \leftarrow flatten(B_i)$; $\bar{\hat{B}}_i \leftarrow flatten(\hat{B}_i)$; $\bar{\mathcal{CS}}_i \leftarrow flatten(\mathcal{CS}_i)$ $\hat{\mathcal{M}}_{o_i} \leftarrow mask(\hat{I}_i^o)$; $A_i = area(\hat{\mathcal{M}}_{o_i})$ $S_i = \{s_{xy} : 1 \leq x, y \leq n\} \leftarrow segment(\hat{I}_i^o)$ **for** each $s_{xy} \in S_i$ **do** $intersectVal \leftarrow area(s_{xy}) \cap A_i$ **if** $intersectVal \geq 10\%$ **then** $tB_{xy} \leftarrow 1$ $tI_{xy} \leftarrow intersectVal \times conf_o(I_i)$ **end****else** $tB_{xy} \leftarrow 0$; $tI_{xy} \leftarrow 0$ **end****end** $tB_i \leftarrow flatten(tB_{xy})$; $t\bar{I}_i \leftarrow flatten(tI_{xy})$ $fc_i \leftarrow \{\mathcal{CS}_i, tI_i, B_i\}$; $fb_i \leftarrow \{\bar{\hat{B}}_i, tB_i, B_i\}$ $FC \leftarrow FC \cup fc_i$; $FB \leftarrow FB \cup fb_i$ **end****return** FC, FB

- Another feature set FC is generated based on confidence value of object mask. If the segment completely overlap with object mask then the confidence value of the segment is same like object mask. Otherwise, it is the fraction of overlapped area. In case of less than 10% overlap the confidence value is 0. This outcome is combined with confidence values of each segment for all test images along ground truth label for corrosion in FC .

The generated feature set FB is then fed into a machine learning classifier such as: support vector machine (SVM), Multilayer Perceptron (MLP) and XGboost using binary outcome of λ_c and λ_o as features and true values as class. Similarly, FC is also fed similar machine learning classifiers using confidence values of 2 models as features and ground truth corrosion value as class.

3.4. Decision for corrosion

As stated before, using trained models several prediction decision for corrosion are made in *decision layer*. They are stated as follow.

- **Segment-level prediction (SLP):** Using λ_c we predict corrosion or non-corrosion of the segmented images in the test set. This prediction is done using the confidence value $conf(s_{xy})$ for segment s_{xy} estimated by λ_c .

If $\text{conf}(s_{xy}) \geq \tau_s$ then, segment has corrosion, otherwise, non-corrosion. Here, τ_s is the minimum confidence value to satisfy the condition for a segment has corrosion and $0 \leq \tau_s, \text{conf}(s_{xy}) \leq 1$.

- **Image-level prediction (ILP):** This means a corrosion prediction for each test image by *aggregating* its segment-level predictions from λ_c . An image, I_i should have $\text{conf}_c(I_i) \geq \tau_I$ to satisfy the condition or corrosion. Where τ_I is the fraction of minimum number of segments should have corrosion among all segments in I_i . τ_i has been determined as the mean value of proportion of corroded segments in all segments in the train set and $0 \leq \tau_I, \text{conf}(s_{xy}) \leq 1$.
- **Industrial object prediction (IOP):** Using λ_o we predict the occurrence and position of target industrial object in test images. This prediction is done using the confidence value $\text{conf}_o(I_i)$ for image I_i estimated by λ_o . If $\text{conf}_o(I_i) \geq \tau_o$ then, image contains the target object, otherwise, false. Here, τ_o is the minimum confidence value to satisfy the condition for occurrence of target object in the image and $0 \leq \tau_o, \text{conf}_o(I_i) \leq 1$.

4. Evaluation

We evaluate **CorrDetector** on real-world images captured by drones. These images are unaltered and used directly in our experimentation. None of existing work in literature used drone images for corrosion detection. Most of these images are collected from web resources [13, 26] or altered/cropped version of images captured by digital camera [4, 5, 7].

The objective of our evaluation is to measure the performance of the ensemble model λ in the **CorrDetector** framework, in comparison with some state-of-the-art CNN models used for corrosion identification.

4.1. Evaluation Domain

We focus on detecting corrosion from telecommunication towers. Thus, we have collected the images of telecommunication towers captured using camera installed in drones. The drones are controlled by operators and they randomly capture different views of telecommunication tower. This differs from many prior works that have conducted evaluations on images collected in controlled settings (i.e. only for the purpose of experimental evaluation) [6, 7].

We have used a total of 573 high-resolution images that contain different views under various lighting conditions of telecommunication towers (see an example in Fig. 4). Each image contains a single tower object and has a 5280×3952 resolution. A telecommunication tower has a complex structure. When random images are captured about it by drones, a high variations is observed in the images (e.g. middle part in Figure 4(b) and bottom part in Figure 4(c)). Also, as seen in 4(a), some part of tower images are overlapped with other objects (e.g. gate) Therefore, it is hard to distinguish which part of the telecommunication tower needs to be inspected for corrosion detection. However, **CorrDetector** can detect such a part correctly and identify the state of corrosion on it.

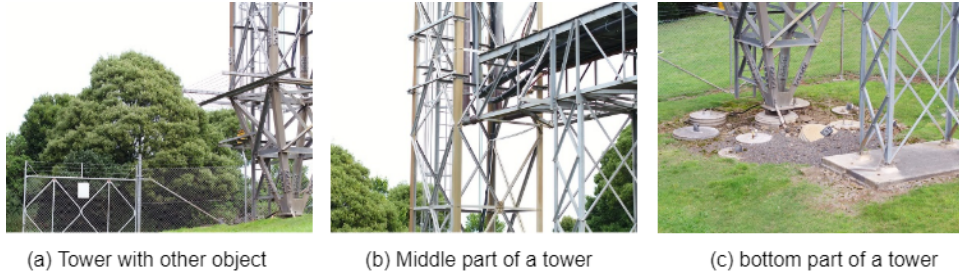


Figure 4: Variations in tower structure in images captured by drones

4.2. Dataset preparation

All the captured images are annotated by experts. Grid-based annotations are performed using the RatSnake [27] software. RatSnake is an annotation tool that is capable of fast annotation of images with polygons, grids or both. Image annotations produced by RatSnake can be exported to various formats. In the grid-based annotation approach, we used $n=16$, that is, each image is segmented and cropped equally to 16×16 segments. Each segment ends up with having a 330×247 resolution (see examples in Fig. 5a). Thus, we have a total of 146,688 segmented image samples ($573 \times 16 \times 16$).

We have also used object annotation for background separation. Object annotation is done using Labelme [23]. LabelMe is a popular annotation tool, where a user can draw both bounding boxes and set of polygon points for segmentation maps. Both online and desktop version of this tool is available. The points of annotated polygon can be saved in JSON or xml format which are used as input for CNN model.

For background separation, authors in [7] first manually cropped the portion of the image having industrial structure. Then, it used that cropped image for segmentation into three different regions, 128×128 , 64×64 , 32×32 . However, in our approach, we have used a 16×16 segmentation on an original image since telecommunication tower views have a complex structure (as in Figure 4). Moreover, the structure of tower is not simple in contrast to a metallic surface as the presence of background can be present within image area covered by the tower. Therefore, it is difficult and time consuming to separately crop only part having corrosion that is proposed in [7].

Our choice of the 16×16 segment size is intuitive as popular CNN models have often used a 224×224 resolution as input image shape [28]. By being scaled at a 224×224 resolution from the 330×247 resolution image segment, we are able to use the image samples to train λ_c nearly in their original resolutions and avoid high distortion due to down-scaling (i.e. from 330×247 scaled to 224×224). Also, the number 16 is chosen to be the maximum granularity level value where we can get an integer number in h (height of segmented image in terms of pixel) which is above 224 and so we can segment according to pixel position in image. RGB (3-channels) colour space is used for forming the input shape of CNN.



Figure 5: Example of Corrosion and non-corrosion segments

4.3. Separation of training and test set

To build any supervised machine learning model, an essential step is to split sample data into train and test sets. Train set is used to build CNN models whereas the test set is utilised for validating the models.

Given the $m=573$ images, we used $k=379$ images (approx. $\frac{2}{3}$ of 573) for training the CNN models for λ_c . A total of the 15,863 segmented images are marked as corrosion by the experts out of the 97,024 ($379 \times 16 \times 16$) segments. Three such sample images are shown in Figure 5a. To avoid a class (i.e. corrosion and non-corrosion) imbalance problem, a total of the 31,726 samples out of 81,161 ($97,024 - 15,863$) were randomly chosen as non-corrosion samples. Thus, we used a total of 47,589 ($15,863 + 2 \times 15,863$) image segments for training as described in Algorithm 1. We used 80%/20% as train/validation set split. Overall, we have a total of 38,701 images for training and 8,888 images for validation in each iteration of CNN model.

During the human annotation phase, as only corrosion segments within the tower structure are annotated by the experts, everything else outside those segments (including background such as trees, grounds, sky and other objects of images, etc) are considered non-corrosion. Some non-corrosion sample segments are presented in Figure 5b.

To evaluate the performance of λ_c , we used 194 ($m - k = 573 - 379 = 194$) images not used for training. That is, we measured the performance of models developed for detecting corrosion in image segment-level using 49,664 image segments ($194 \times 16 \times 16$).

To train λ_o , annotated polygonal mask of $m=379$ images are used for training Mask R-CNN model. The model is evaluated using the remaining 194 images. During the training, we used 70%/30% split that is, 265 image for training and 114 images for validation. Here we used ResNet101 as backbone network (ResNet101 is 101 layers deep). We prefer this split over 80%/20% which we used for λ_c so we can get higher number of images in validation.

4.4. Evaluation Metrics

We evaluate the performance of individual CNNs and the ensemble model, λ , using different performance measures over test set. We use accuracy ($Acc.$), precision (P), recall (R) and F1-score ($F1$), obtained from true positive (TP), false positive (FP), true negative (TN) and false negative (FN) values from the classification result (i.e. confusion matrix) over test set:

To evaluate λ_o we also measure Intersection over Union (IoU) [29] for I_i as in equation 4.

$$IOU(I_i) = \frac{Area(\hat{\mathcal{M}}_{o_i} \cap \mathcal{M}_{o_i})}{Area(\hat{\mathcal{M}}_{o_i} \cup \mathcal{M}_{o_i})} \quad (4)$$

This computes the amount of overlap between the detected and the ground truth polygonal masks. Similar measure is defined for bounding box annotation also (Equation 5).

$$IOU(I_i) = \frac{Area(\hat{\mathcal{BB}\mathcal{O}\mathcal{X}}_{o_i} \cap \mathcal{BB}\mathcal{O}\mathcal{X}_{o_i})}{Area(\hat{\mathcal{BB}\mathcal{O}\mathcal{X}}_{o_i} \cup \mathcal{BB}\mathcal{O}\mathcal{X}_{o_i})} \quad (5)$$

Figure 6 shows the demonstration for computing IoU for mask and Bbox.

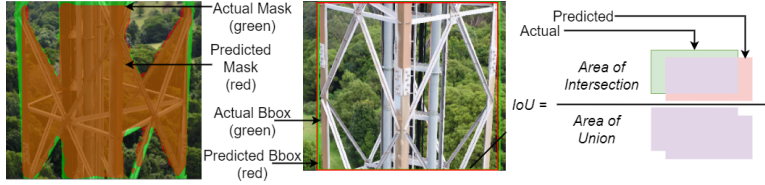


Figure 6: The process of computing IoU using ground truth and predicted value

To measure the performance of object position detection in I_i , if $IOU(I_i) \geq IOU_{th}$ then it is considered that the target object mask $\hat{\mathcal{M}}_{o_i}$ estimated the position in the object T in I_i accurately (true positive (TP) case). Otherwise, this is considered as false positive (FP). Here $0 \leq IOU_{th} \leq 1$ and generally, TP is considered when $IOU_{th} > 0.5$. Thus, using TP , FP it is possible to compute precision using the outcome from all test images.

Object detectors normally use Average precision(AP) as metric to measure the performance of the detection. AP is the average over multiple IOU_{th} . For example, AP for IOU_{th} values from 0.5 to 0.75 with a step size of 0.05. We also used AP for for evaluating λ_o using IOU values for object mask and bounding boxes.

We use human annotations as gold standards for computing accuracy across all models.

4.5. Compared State-of-the-art CNN Models

Our ensemble model λ is also compared with some state-of-the-art deep learning models described in Section 2. In particular, we compare λ_c with two models (i.e. Corrosion5 and Corrosion7) specifically designed for corrosion detection in [7] using cropped image. Further, we compare λ_c with four pre-trained models through transfer learning, InceptionV3 [30], MobileNet [31], Rsetnet50 [32], and Vgg16 [24]. Corrosion5 is a simpler version of Corrosion7 described in Table 2 with 3 convolution layers and 2 fully connected layers. Corrosion5 and Corrosion7 in [7], used different kernel shapes and authors have not clearly explained the reason for choosing such kernel shapes. Our model, λ_c as described

in Table 1 is a 5 layered CNN with the first FC has 128 neurons followed by the binary classification layer (i.e. corrosion or not) with 2 neurons. To evaluate how corrosion detection performs with a simpler structure, we also develop a simple CNN with only one convolution layer and two fully-connected layers.

4.6. Evaluation of developed models: λ_c , λ_o and λ

The two CNN models λ_c and λ_o are trained and evaluated in multiple iterations and various configurations on two NVIDIA Tesla P100-PCIE-12GB GPUs on CUDA with four Intel Gold 6140 18-core processors. Finally, λ is developed using the outcome of λ_c and λ_o . In this section, the model development process and evaluation outcomes are described.

4.6.1. Training and Evaluation for Corrosion Detection Model λ_c

As stated in section 3.3.1, λ_c is developed to predict corrosion or not as a binary classification problem. Thus, the binary cross-entropy is used as a loss function.

To train λ_c , different configurations of hyper-parameters are used such as input dimensions for sample images (e.g. 128×128 , 200×200 , 220×220 , 224×224), batch size (e.g. 16, 32, 64, 128) and number of epochs (10, 20, 30, 50, 100). Moreover, rotation, shear range, zoom range, width and height shift and horizontal flips are used during input data generation [28].

The model with the best outcome in terms of performance measure (e.g. low training loss) are retained. Finally, all the compared CNN models are trained using same configurations (i.e. batch size=64, number of epoch =30 and input image shape 224×224). For the transfer learner models, the pre-trained weights are fine-tuned to re-train with generated training set.

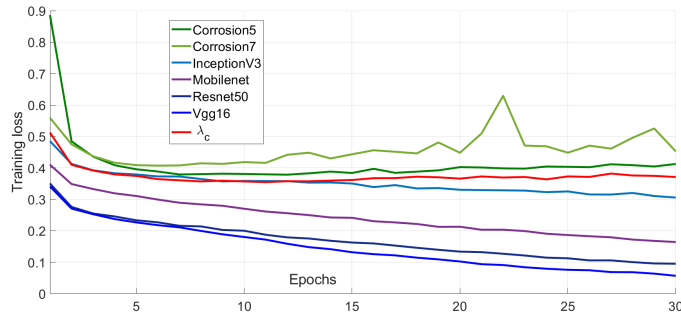


Figure 7: Training loss for the seven CNN models compared

The learning curves based on the the same loss function across eight models during training are presented in Figure 7. As observed, all the models were converged after around 30 epochs. The training loss was lower in four pre-trained models - InceptionV3, MobileNet, Restnet50 and VGG16. Our model, λ_c , showed stability than Corrosion5 and Corrosion7. The training loss was higher in Corrosion5 and Corrosion7 [7] than λ_c and four pre-trained models.

Moreover, Corrosion5 had a high loss value at the beginning and Corrosion7 was unstable (as shown between epoch 20 and 30). The loss value for λ_c after 30 iterations was 0.3702. The pre-trained model converged very quickly and the training losses are lower than λ_c . The lowest loss after 30 iterations was 0.0567 obtained in Vgg16. However, though the pre-trained models performed well in training data, lower accuracy were observed on test data (discussed below).

In the evaluation, we first measure the performance of λ_c without integrating λ_o . Due to variations in tower images and corrosion from unknown sources the evaluation outcome from λ_c can generate many false positives (FPs). The reason of building λ_o is to suppress those FPs so that detected corrosion segments remain in tower object. Therefore, each of image is annotated separately for building λ_c and λ_o . We have used $\tau_s = 0.5$ (for λ_c) as it is a general standard value for CNN in binary classification [6]. τ_s is minimum confidence value to satisfy the condition for a segment, s_{xy} has corrosion and $0 \leq \tau_s, \text{conf}(s_{xy}) \leq 1$.

Table 3: Performance comparison for segment-level and image-level prediction

CNN model	Acc.(%)		P(%)		R(%)		F1(%)	
	SLP	ILP	SLP	ILP	SLP	ILP	SLP	ILP
Simple CNN	58.17	37.52	22.31	38.36	34.58	88.41	27	54
Our model, λ_c	86.28	92.50	53.42	96.01	85.41	95.91	66	98
Corrosion5 [7]	78.24	62.48	65.67	65.92	44.7	91.7	53	77
Corrosion7 [7]	81.67	68.41	60.02	70.76	52.60	94.05	56	80
InceptionV3	81.58	66.31	42.34	69.10	63.93	92.94	51	79
Mobilenet	73.86	61.76	43.22	64.30	25.18	92.47	32	76
Resenet50	75.04	63.33	44.71	65.61	31.23	93.13	37	77
Vgg16	77.97	68.88	51.81	70.20	58.96	94.01	55	80

The evaluation results in terms of the evaluation metrics (i.e accuracy, precision, recall and F1-score) on segment-level prediction (SLP) and image-level prediction (ILP) are presented in Table 3. As seen, our model, λ_c , already outperforms the other seven CNN models in terms of all the performance metrics (highlighted in yellow) except precision in SLP. The simple CNN performs the worst which confirms that a single CNN layer may not be sufficient for corrosion detection. In the pre-trained models, the accuracy of InceptionV3 is turned to be better than the others but Vgg16 is better in terms F1 due to the higher precision value.

In terms of accuracy, recall and F1-score λ_c is also the best. The two models, Corrosion5 and Corrosion7, in [7] did not perform well on our test data. Four pre-trained models did not perform so well in test data even though they were outstanding in train data.

The prediction results of image I_i , matrix B_i (i.e SLP) in segment-level are aggregated to detect corrosion for ILP. Out of 573 annotated images used in training and testing in total 10% segments are marked as corrosion by the human experts. Therefore, we used the threshold, $\tau_I = 0.1$. That is, given an image, if more than 10% segments are marked as corrosion by a CNN model,

then this image is considered to be corrosion. Using this notion, the performance of ILP for 194 images are calculated which is presented in Table 3. As seen, λ_c showed 92.5% in Accuracy and 98% in F1-score. This shows the effectiveness of our proposed model over the other state-of-the-art and pre-trained models we compared with. However, due to high number of false positives (FPs) the precision in SL was low. To improve this and eliminate FPs happened outside tower structure, we developed λ_o and then combined it in ensemble model λ .

4.6.2. Training and Evaluation for Object Identification Model λ_o

We have used pre-trained weights of COCO model [33] to train λ_o . The pre-trained network can classify images into 1000 known object categories. To increase the sample size we have used image augmentation such as rotation, flip and skew. Here we also trained multiple networks with various configurations of hyper parameters. Finally, we used 512×512 as input image dimension and batch size 64. The network is configured as single object classification problem with 2 classes - tower and background. Different loss metrics reported by the network during training phase is shown in Figure 8. As observed, the trained model converged after around 120 epochs. Thus, we use this model as λ_o for tower classification.

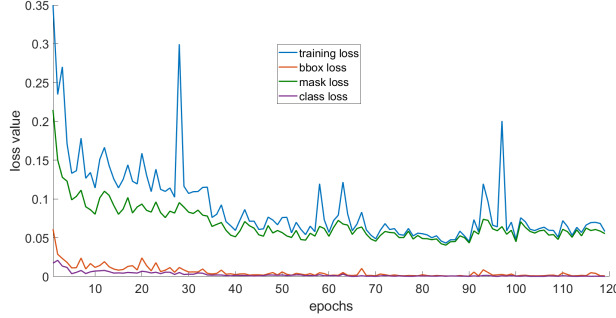


Figure 8: Loss metrics observed for λ_o

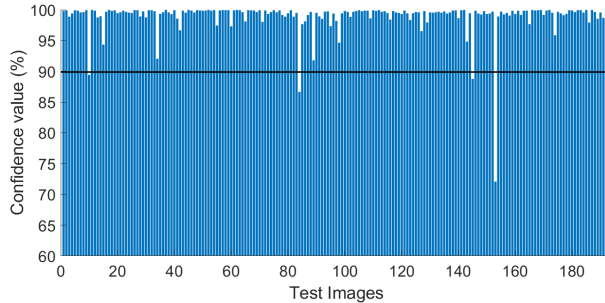


Figure 9: Confidence value of tower object recognition over 194 test images

We have used $\tau_o = 0.9$, that is, the confidence value over 90% is considered as correct recognition. Based on this condition in 190 out of 194 images tower is classified with confidence ≥ 0.9 and while the other 4 were below the threshold (see Figure 9), therefore object recognition accuracy is 98%.

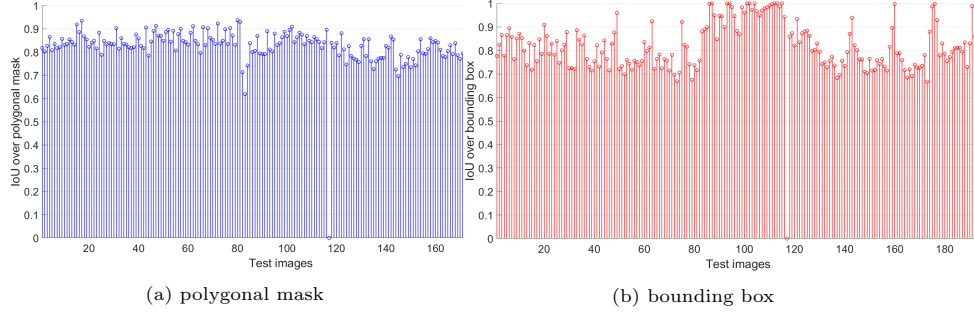


Figure 10: IoU values

The IoU values for mask and bbox according to Equation 4 and 5 are also computed for 194 test images which is presented in Figure 10a and 10b. As observed from IoU values for both processes, the mask for only one image was not predicted correctly. Other images, satisfies the condition for true positive for $IOU \geq 0.5$ for both mask and bounding box overlap. Table 4 shows the performance of λ_o using precision (IOU_{th} values) from 0.5 to 0.75 with a step size of 0.05 [29] and final AP value. The th value is considered till 0.75 as the precision value significantly deteriorated after that. In both cases λ_o showed very high AP value (98.11% for polygonal mask and 94.42% for bounding box).

Table 4: Precision and Average Precision (AP) using IoU over mask and bounding box

IoU	$IoU_{0.5}$	$IoU_{0.55}$	$IoU_{0.6}$	$IoU_{0.65}$	$IoU_{0.7}$	$IoU_{0.75}$	AP
P_{mask}	99.49%	99.49%	99.49%	98.97%	98.45%	92.78%	98.11%
P_{bbox}	99.49%	99.49%	99.49%	99.49%	94.85%	73.71%	94.42%

4.6.3. Training and Evaluation for the ensemble model, λ

As presented in Table 3 we did not obtain good precision for λ_c due to higher false positives (FPs). To improve the precision in λ_c (i.e. minimise FPs) we developed the ensemble model, λ , by combining outcomes of λ_c and λ_o . As described in Algorithm 2, two feature sets (FC and FB) are generated using binary outcomes and confidence values of λ_c and λ_o . Both FC and FB (presented in Algorithm 2) are randomised and fed into the selected machine learning models. The results obtained from both feature sets over the best performing machine learning classifiers are presented in Table 5.

We observed higher precision values as well as accuracy, recall and F1 in λ than λ_c (which was 53.2% before) over all 3 classifiers (MLP, SVM and XG-Boost). For, FB all classifiers showed same performance in terms of accuracy,

Table 5: Performance of λ using *FB* and *FC* as feature set and different ML classifier

Ensemble model	Acc.(%)		P(%)		R(%)		F1(%)	
	FB	FC	FB	FC	FB	FC	FB	FC
MLP	93.80	83.25	88.00	92.30	93.80	83.20	90.80	86.80
SVM	93.80	83.70	88.00	92.30	93.80	83.70	90.80	87.10
XGBoost	93.80	86.29	88.00	92.10	93.80	86.30	90.80	88.70

precision, recall and F1-score. However, the performance of XGBoost was the best among all in *FC* in terms of accuracy and F1-score. In λ we observed 8.72% improvement accross all 3 classifiers in accuracy over the SLP in λ_c . The final evaluation outcome from λ , provides evidence that **CorrDetector** is an effective model for corrosion detection. The ensemble model over multiple CNNs can detect corrosion on real-world images with 93.8% accuracy and with 88% precision and 90.8% F1-score. Our evaluation results show the validity of our primary motivation that utilising an ensemble of CNN models can be effectively used for corrosion detection in drone images of complex industrial structure.

5. Conclusion

We have presented **CorrDetector**, an ensemble AI framework underpinned by CNN models for structural identification and corrosion detection in civil engineering settings. Our approach relies on standard approaches to drone managed image capture technologies used in the risk-based maintenance philosophy. This industry conforming approach makes **CorrDetector** applicable in standard working practises where images are used to carry out in-person inspections due to either safety concerns or inaccessibility. Our approach provides engineers with advanced indication of which images may contain sufficient corrosion to warrant maintenance intervention. This in turn provides an opportunity for fine tuning analysis and assessment further along the value chain of the maintenance life cycle by allowing resources to be directed only to those structures highlighted by **CorrDetector**. This opportunity can greatly reduce financial costs and extend the resources of engineers to consider far more images than would otherwise be possible in a human based analysis.

We evaluated **CorrDetector** via empirical evaluations with state-of-the-art that also utilise AI techniques for structural corrosion analysis. We demonstrated that our approach is a significant improvement and achieved an overall success rate in excess of 92%. This level of success indicates a level of efficacy that will allow our approach to provide the foundations for building engineering analysis tools, especially in the area of supporting telecommunication tower safety and maintenance life cycle services. Future work will explore applying **CorrDetector** in a broader range of structures and settings.

References

- [1] F. Fang, L. Li, Y. Gu, H. Zhu, J.-H. Lim, A novel hybrid approach for crack detection, *Pattern Recognition* (2020) 107474.
- [2] R. Javaherdashti, Microbiologically influenced corrosion (mic), in: *Microbiologically Influenced Corrosion*, Springer, 2017, pp. 29–79.
- [3] R. Javaherdashti, How corrosion affects industry and life, *Anti-corrosion methods and materials* (2000).
- [4] L. Petricca, T. Moss, G. Figueroa, S. Broen, Corrosion detection using ai: a comparison of standard computer vision techniques and deep learning model, in: *Proceedings of the Sixth International Conference on Computer Science, Engineering and Information Technology*, volume 91, 2016, p. 99.
- [5] C. Fernández-Isla, P. J. Navarro, P. M. Alcover, Automated visual inspection of ship hull surfaces using the wavelet transform, *Mathematical Problems in Engineering* 2013 (2013).
- [6] Y.-J. Cha, W. Choi, G. Suh, S. Mahmoudkhani, O. Büyüköztürk, Autonomous structural visual inspection using region-based deep learning for detecting multiple damage types, *Computer-Aided Civil and Infrastructure Engineering* 33 (2018) 731–747.
- [7] D. J. Atha, M. R. Jahanshahi, Evaluation of deep learning approaches based on convolutional neural networks for corrosion detection, *Structural Health Monitoring* 17 (2018) 1110–1128.
- [8] M. Jahanshahi, S. Masri, Effect of color space, color channels, and sub-image block size on the performance of wavelet-based texture analysis algorithms: An application to corrosion detection on steel structures, in: *Computing in Civil Engineering* (2013), 2013, pp. 685–692.
- [9] M. R. G. Acosta, J. C. V. Díaz, N. S. Castro, An innovative image-processing model for rust detection using perlin noise to simulate oxide textures, *Corrosion Science* 88 (2014) 141–151.
- [10] H. Son, N. Hwang, C. Kim, C. Kim, Rapid and automated determination of rusted surface areas of a steel bridge for robotic maintenance systems, *Automation in Construction* 42 (2014) 13–24.
- [11] J. Gu, Z. Wang, J. Kuen, L. Ma, A. Shahroudy, B. Shuai, T. Liu, X. Wang, G. Wang, J. Cai, et al., Recent advances in convolutional neural networks, *Pattern Recognition* 77 (2018) 354–377.
- [12] P. P. Jayaraman, A. R. M. Forkan, A. Morshed, P. D. Haghighi, Y.-B. Kang, *Healthcare 4.0: A review of frontiers in digital health*, *Wiley Interdisciplinary Reviews: Data Mining and Knowledge Discovery* 10 (2020) e1350.

- [13] V. Hoskerc, Y. Narazaki, T. Hoang, B. Spencer Jr, Vision-based structural inspection using multiscale deep convolutional neural networks, arXiv preprint arXiv:1805.01055 (2018).
- [14] X. Zheng, W. Chen, Y. You, Y. Jiang, M. Li, T. Zhang, Ensemble deep learning for automated visual classification using eeg signals, *Pattern Recognition* 102 (2020) 107147.
- [15] Y.-J. Cha, W. Choi, O. Büyüköztürk, Deep learning-based crack damage detection using convolutional neural networks, *Computer-Aided Civil and Infrastructure Engineering* 32 (2017) 361–378.
- [16] S. H. Hanzaei, A. Afshar, F. Barazandeh, Automatic detection and classification of the ceramic tiles’ surface defects, *Pattern Recognition* 66 (2017) 174–189.
- [17] J. Liu, H. Li, R. Wu, Q. Zhao, Y. Guo, L. Chen, A survey on deep learning methods for scene flow estimation, *Pattern Recognition* 106 (2020) 107378.
- [18] M. M. R. Taha, A. Noureldin, J. L. Lucero, T. J. Baca, Wavelet transform for structural health monitoring: A compendium of uses and features, *Structural Health Monitoring* 5 (2006) 267–295.
- [19] R. M. Pidaparti, Structural corrosion health assessment using computational intelligence methods, *Structural Health Monitoring* 6 (2007) 245–259.
- [20] V. Pakrashi, F. Schoefs, J. B. Memet, A. O’Connor, Roc dependent event isolation method for image processing based assessment of corroded harbour structures, *Structure and Infrastructure Engineering* 6 (2010) 365–378.
- [21] K. He, G. Gkioxari, P. Dollár, R. Girshick, Mask r-cnn, in: *Proceedings of the IEEE international conference on computer vision*, 2017, pp. 2961–2969.
- [22] C. Dagli, T. S. Huang, A framework for grid-based image retrieval, in: *Proceedings of the 17th International Conference on Pattern Recognition*, 2004. ICPR 2004., volume 2, IEEE, 2004, pp. 1021–1024.
- [23] B. C. Russell, A. Torralba, K. P. Murphy, W. T. Freeman, Labelme: a database and web-based tool for image annotation, *International journal of computer vision* 77 (2008) 157–173.
- [24] K. Simonyan, A. Zisserman, Very deep convolutional networks for large-scale image recognition, arXiv preprint arXiv:1409.1556 (2014).
- [25] T.-Y. Lin, P. Dollár, R. Girshick, K. He, B. Hariharan, S. Belongie, Feature pyramid networks for object detection, in: *Proceedings of the IEEE conference on computer vision and pattern recognition*, 2017, pp. 2117–2125.

- [26] F. Bonnin-Pascual, A. Ortiz, Corrosion detection for automated visual inspection, in: *Developments in Corrosion Protection*, IntechOpen, 2014.
- [27] D. K. Iakovidis, T. Goudas, C. Smailis, I. Maglogiannis, Ratsnake: a versatile image annotation tool with application to computer-aided diagnosis, *The Scientific World Journal* 2014 (2014).
- [28] A. Gulli, S. Pal, *Deep Learning with Keras*, Packt Publishing Ltd, 2017.
- [29] H. Rezatofighi, N. Tsoi, J. Gwak, A. Sadeghian, I. Reid, S. Savarese, Generalized intersection over union: A metric and a loss for bounding box regression, in: *Proceedings of the IEEE Conference on Computer Vision and Pattern Recognition*, 2019, pp. 658–666.
- [30] S. M. Sam, K. Kamardin, N. N. A. Sjarif, N. Mohamed, et al., Offline signature verification using deep learning convolutional neural network (cnn) architectures googlenet inception-v1 and inception-v3, *Procedia Computer Science* 161 (2019) 475–483.
- [31] A. G. Howard, M. Zhu, B. Chen, D. Kalenichenko, W. Wang, T. Weyand, M. Andreetto, H. Adam, Mobilenets: Efficient convolutional neural networks for mobile vision applications, *arXiv:1704.04861* (2017).
- [32] K. He, X. Zhang, S. Ren, J. Sun, Deep residual learning for image recognition, in: *Proceedings of the IEEE conference on computer vision and pattern recognition*, 2016, pp. 770–778.
- [33] W. Abdulla, Mask R-CNN for object detection and instance segmentation on keras and tensorflow, https://github.com/matterport/Mask_RCNN, 2017.